XLVI CILAMCE
VITÓRIA - ES - BRAZIL - 2025
XLVI IBERO-LATIN AMERICAN CONGRESS ON COMPUTATIONAL METHODS IN ENGINEERING

Analysis of extreme temperature under climate change and structural impacts on infrastructure

Mariana de A. Silva[1], Francisco E. Júnior[1]

[1]*Dept. of Civil Engineering, University of Brasília*
Darcy Ribeiro Campus, 70910-900, Brasília, DF, Brazil
mari.alvarenga96@gmail.com, fejr@unb.br

Abstract. The global rise in air temperatures due to climate change poses increasing challenges for the durability and performance of transportation infrastructure. This study evaluates the effects of surface temperatures on concrete pavements by combining meteorological data analysis with surface temperature estimation and curling stress calculation. Hourly weather data from São Paulo, Brazil, were processed using an energy balance model to estimate pavement surface temperature. Seasonal statistics characterized long-term trends, while thermal gradients were used to estimate curling stresses in rigid pavements. Additionally, Dynamic Time Warping (DTW) and peak prominence analysis were applied to compare hourly summer series of temperature and stress, capturing both magnitude and morphological changes over time. Results show a consistent upward trend in seasonal surface temperatures and pavement stresses. Peak prominence and Dynamic Time Warping (DTW) analyses of summer series identified morphological and magnitude changes in the events, with years such as 2013 and 2020 standing out for distinctive patterns. Results highlight the importance of incorporating both long-term warming and seasonal pattern changes into pavement design and maintenance strategies to ensure structural resilience.

Keywords: Pavement surface temperature, Thermal stresses, Dynamic Time Warping.

1 Introduction

Climate change has emerged as one of the most pressing global challenges, with profound impacts across environmental, economic, and social dimensions. Among its multiple consequences, the intensification of extreme temperature events has become a critical concern for infrastructure systems, particularly in the transportation sector. In the context of infrastructure, specifically on pavements, whether asphalt or concrete, are continuously subjected to environmental loading, and prolonged exposure to elevated temperatures can accelerate deterioration processes, reduce service life, and increase maintenance demands.

In rigid pavements, daily and seasonal temperature variations generate thermal gradients along the slab thickness, producing curling stresses. When extreme temperature events occur more frequently or with higher intensity, these stresses can reach magnitudes that compromise structural integrity, resulting in phenomena such as thermal cracking. Consequently, accurate prediction of pavement surface temperature under changing climatic conditions is essential for both design and performance assessment.

Previous studies have proposed empirical and physics-based models to estimate surface temperatures based on meteorological inputs, solar radiation, and material properties. Notably, the model by Solaimanian and Kennedy [1], grounded in the surface energy balance, allows for the incorporation of location-specific climatic data into temperature estimations. This approach, combined with statistical modeling of extremes, enables engineers to evaluate not only typical conditions but also rare and potentially critical thermal scenarios.

In this context, the present study aims to analyze long-term trends in extreme pavement surface temperatures using historical meteorological data; quantify the curling stresses induced in concrete slabs under such thermal loads; and investigate the morphological evolution of thermal and stress time series using the Dynamic Time Warping (DTW) technique.

2 Background

2.1 Predicting pavement surface temperature

Concrete pavements are continuously exposed to daily and seasonal thermal variations, which result in repeated cycles of heating and cooling at both the surface and subsurface layers. These thermal fluctuations generate temperature gradients along the slab thickness, leading to internal stresses due to the differential expansion and contraction of materials, especially when there is a significant difference between the surface and base temperatures. Such gradients can contribute to thermal cracking, slab curling, and progressive structural deterioration, compromising the long-term performance of the pavement.

Given the significance of this phenomenon, it becomes essential to determine the surface temperature to assess the influence of environmental conditions on the structural behavior of the pavement. In this way, the present study adopts the methodology proposed by Solaimanian and Kennedy [1], which is based on the energy balance at the pavement–atmosphere interface. This approach allows the estimation of the pavement surface temperature using climatic data, geographical location, and material thermal properties.

In this model, the net rate of heat transfer at the pavement surface is defined by the following expression:

$$q_{net} = q_s + q_a - q_c - q_k - q_r = 0 \tag{1}$$

where q_s is the energy absorbed from direct solar radiation, q_a is the energy absorbed from diffuse atmospheric radiation, q_c is the energy exchanged with the air by convection, q_k is the energy transferred by conduction with the underlying pavement layers and q_r is the energy emitted from the surface through thermal radiation.

The energy absorbed from direct solar radiation, q_s, can be calculated as

$$q_s = \alpha R_i \tag{2}$$

where α is the surface absorptivity and R_i is the incident solar radiation. The incident solar radiation R_i depends on the angle between the direction of the normal to the surface receiving radiation and the direction of the solar radiation, i.e.

$$R_i = R_0 \tau_a^m \cos i \tag{3}$$

In the equation presented above, i is the angle between the normal to the surface and the direction of radiation. R_0 is the solar constant (approximately 1394 W/m²), m denotes the relative air mass, and τ_a is the transmission coefficient for unit air mass. The value of τ_a varies depending on sky conditions, ranging from 0.81 on a clear day to 0.62 on a cloudy one and the relative air mass is approximately equal to $1/\cos z$, where z is the zenith angle. This angle depends on the latitude, ϕ, the hour angle, h, and the solar declination δ_s, as shown in Eq. 4. For horizontal surfaces $\cos i = \cos z$.

$$\cos z = \sin\phi \sin\delta_s + \cos\delta_s \cos\phi \tag{4}$$

Regarding atmospheric radiation, the energy absorbed by the pavement surface can be estimated using the empirical expression developed by Geiger [2], as cited in Solaimanian and Kennedy [1]:

$$q_a = \varepsilon_a \sigma T_a^4 \tag{5}$$

where σ is the Stefan–Boltzmann constant ($5.68 \cdot 10^{-8}\ Wm^{-2}K^{-4}$), T_a is the air temperature, and ε_a is given by:

$$\varepsilon_a = G - J(10^{-\rho P}) \tag{6}$$

In this expression, G, J, and P are constants (0.77, 0.28, and 0.074, respectively), and ρ is the water vapor pressure in mmHg.

The conductive heat flux is approximated by:

$$q_k = -k \frac{T_d - T_s}{d} \tag{7}$$

where k is the thermal conductivity, T_s is the pavement surface temperature, d is the depth, and T_d is the temperature at depth d.

The radiation emitted by the pavement surface is calculated according to Eq. 8, as a function of the emissivity ε.

$$q_r = \varepsilon \sigma T_s^4 \tag{8}$$

Finally, the convective heat flux between the pavement and the surrounding air is given by:

$$q_c = h_c(T_s - T_a) \tag{9}$$

where h_c is the convective heat transfer coefficient, which depends on surface geometry, wind speed, and fluid properties. In this study, h_c ($W/m°C^{-1}$) is estimated using the correlation proposed by Qin and Hiller [3]:

$$h_c = 5.6 + 0.332 Re^{0.5} \, \mathrm{Pr}^{1/3} \frac{K_{air}}{L} \tag{10}$$

For air, the thermal conductivity $K_{air} = 0.027$ and the Prandtl number Pr is 0.7. Considering air flow over a flat plate, $L = 0.15$. The Reynolds number Re is defined by Eq. 11 as a function of the wind speed, v, and the kinematic viscosity, υ, which is typically assumed to be $16.01 \cdot 10^{-6}\ m^2 s^{-1}$.

$$Re = vL/\upsilon \tag{11}$$

2.2 Estimate of curling stresses in finite slab

According to Huang [4], the thermally induced stresses at the center of a finite slab can be estimated using Eq. 12, under the assumption that temperature varies linearly through the slab thickness. This is an approximation, since the actual temperature distribution is nonlinear, as noted by Huang [4] and demonstrated by Qin and Hiller [3].

$$\sigma_x = \frac{E \alpha_t \Delta t}{2(1-\nu^2)}\left(C_x + \nu C_y\right), \quad \sigma_y = \frac{E \alpha_t \Delta t}{2(1-\nu^2)}\left(C_y + \nu C_x\right) \tag{12}$$

In the equation above, E denotes the modulus of elasticity of concrete, α_t is the coefficient of thermal expansion of concrete, ν is Poisson's ratio, and C_x and C_y are correction factors associated with the infinite slab assumption. They depend on the slab lengths L_x and L_y as well as on the radius of relative stiffness, defined as

$$l = \left[\frac{E d^3}{12(1-\nu^2)k_s}\right]^{0.25} \tag{13}$$

where d is the thickness of the slab and k_s is the modulus of subgrade reaction.

2.3 Dynamic Time Warping (DTW)

Dynamic Time Warping (DTW) is a widely used technique for measuring similarity between two time series that may be misaligned or exhibit temporal distortions. Unlike traditional metrics such as linear normalization, DTW allows for non-linear alignment of sequences, minimizing the cumulative distance between matching points (Sakoe and Chiba [5]). This makes it particularly valuable in fields like pattern recognition, time series classification, data mining, and biomedical signal processing. The following presents the mathematical definitions of the DTW technique, as described by Müller [6].

Given a feature space denoted by $\mathcal{F}$ and two time series $X := (x_1, \ldots, x_n)$ and $Y := (y_1, \ldots, y_m)$, which x_n, $y_m \in \mathcal{F}$ for $n \in [1\colon N]$ and $m \in [1\colon M]$. To compare two different features x, $y \in \mathcal{F}$, a local cost measure, also referred to as local distance measure, is required, defined as

$$c : \mathcal{F} \times \mathcal{F} \to \mathbb{R}_{\geq 0}. \tag{14}$$

A warping path, $p = (p_1, \ldots, p_L)$, where $p_l = (n_l, m_l)$, which must satisfy boundary, continuity, and monotonicity constraints, defines the alignment between two time series by specifying how their elements are matched to one another. The total cost $c_p(X, Y)$ of p between X and Y with respect to the local cost measure c is defined as

$$c_p(X, Y) := \sum_{l=1}^{L} c(x_{n_l}, y_{m_l}). \tag{15}$$

In this way, a path p^* is an optimal warping path when has minimal total cost among all possible warping paths. As a result, DTW distance between X and Y is defined as the total cost of p^*:

$$DTW(X,Y) := c_{p^*}(X,Y) = \min c_p(X,Y) \tag{16}$$

To compute this distance efficiently, a dynamic programming approach is applied by constructing a cumulative cost matrix $D(n,m)$, where each entry stores the minimal cost to align $X_{1:n}$ and $Y_{1:m}$. The optimal alignment path can be retrieved by computing in reverse order of the indices starting with the endpoint $p_L = (N,M)$. If the current point is $p_l = (n,m)$ and $(n,m) = (1,1)$, the algorithm terminates, since $l = 1$. Otherwise:

$$p_{l-1} := \begin{cases} (1,m-1), if\ n = 1 \\ (n-1,1), if\ m = 1 \\ argmin\{D(n-1,m-1), D(n-1,m), D(n,m-1)\} \end{cases} \tag{17}$$

In case of multiple predecessors have the same minimal cost, the lexicographically smallest pair is selected.

3 Methodology

The methodology adopted in this study was based on the collection and analysis of meteorological data provided by the Brazilian National Institute of Meteorology (INMET) [7], specifically from weather station A701, located in São Paulo at coordinates 23°29'46.6"S, 46°37'12.2"W. The analyzed period extends from the station's installation on July 24, 2006, to March 31, 2025, encompassing nearly 19 years of hourly records.

Using historical data on air temperature, relative humidity, wind speed, and cloud cover, the components of the surface energy balance equation for the pavement were estimated and assuming thermal equilibrium, the net heat flux at the surface was set to zero.

By replacing each term with known physical expressions and incorporating both historical data and the variables listed in Table 1, a polynomial equation dependent on the surface temperature and the temperature at a given depth d was obtained. This equation was solved numerically using MATLAB scripts, enabling the determination of the surface and subsurface temperatures that satisfy the thermal equilibrium condition.

Table 1. Case study variables

Thermal analysis variables	Value	Stress analysis variables	Value
α	0.725[a]	E	35 GPa
k	2.20 $Wm^{-1}K^{-1}$ [a]	α_t	$8 \cdot 10^{-6}$/ºC [b]
d	0.22 m	ν	0.15
ε	0.90[a]	L_x	5.0 m
-	-	L_y	3.5 m

[a]: suggested in [8]; [b]: suggested in [9]

Based on the surface temperature and the resulting thermal gradient (ΔT), the thermal stresses induced in the concrete slab were estimated using a simplified bending model for slabs on a continuous foundation, considering typical concrete properties and geometric features, as also shown in Table 1.

Furthermore, in order to deepen the understanding of the thermal behavior, an additional time series analysis code was developed in MATLAB. This module implements an application of the Dynamic Time Warping (DTW) algorithm to compare thermal and stress time series patterns across different years and seasons, accounting distortions and capturing the structural similarity between the profiles.

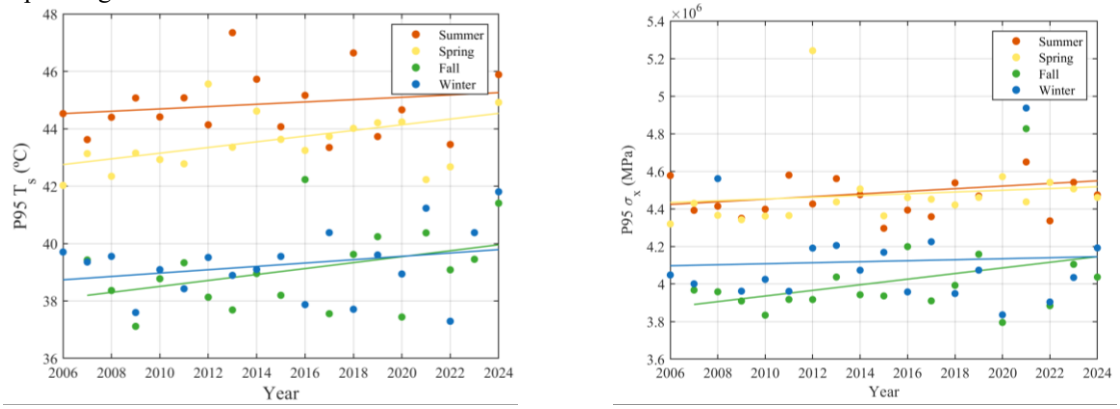
Complementary statistical analyses were also performed, including trend analysis of surface temperature throughout the studied period and correlation between meteorological input variables (air temperature, humidity, wind, cloudiness, and seasonality) and the estimated pavement surface temperatures, with the goal of identifying the most influential environmental parameters driving pavement heating.

4 Results and discussion

Figure 1 illustrate the temporal evolution of 95th percentile for T_s and σ_x series across seasons from 2006 to

2024. A positive linear trend is observed for all seasons in the two indicators, with summer showing mostly the highest absolute values.

Combining the results from Fig. 1 with the regression slopes in Table 2, it becomes evident that although summer presents the highest absolute values for both T_s and σ_x, the greatest rates of increase over the 2006–2024 period do not occur in this season. Additionally, the similar patterns observed in the graphs for both variables indicate a strong temperature–stress coupling, whereby the long-term warming trend is likely driving the corresponding increase in tensile stress.



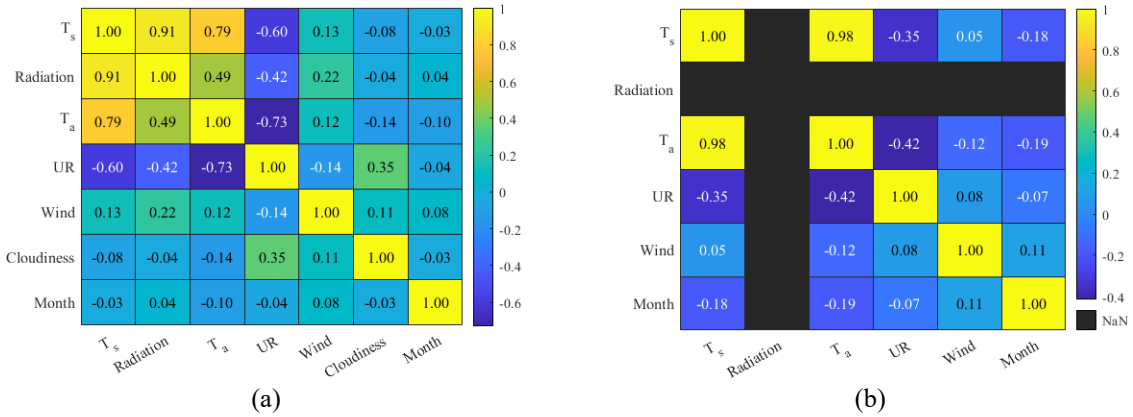
(a) (b)

Figure 1. Temporal trend of 95th percentile (a) for T_s and (b) for σ_x

Table 2. Regression slopes

Season	T_s slopes	σ_x slopes
Summer	0.0406	$6.996 \cdot 10^3$
Spring	0.0991	$4.629 \cdot 10^3$
Fall	0.1036	$14.957 \cdot 10^3$
Winter	0.0585	$2.673 \cdot 10^3$

The relationship between surface temperature (T_s) and climatic variables was analyzed using Pearson correlation coefficients (Figure 2) for morning and evening periods. Strong correlations are observed between T_s, global solar radiation, and air temperature, indicating that surface temperature is predominantly driven by radiative heat flux and atmospheric conditions. Conversely, relative humidity (UR) is negatively correlated with T_s, reinforcing its role in thermal moderation, as higher humidity typically implies cloudier skies and lower solar input.



(a) (b)

Figure 2. Correlation matrix for (a) the morning period and (b) the evening period

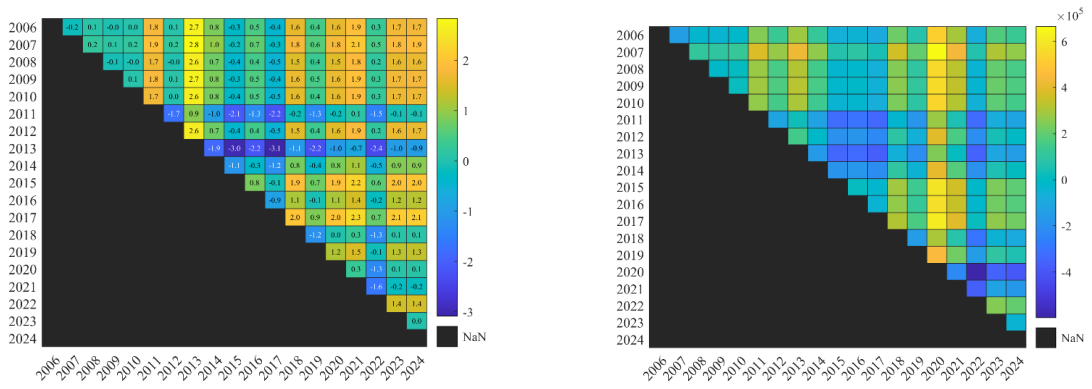
Figure 3 shows heat maps of the average peak prominence differences for pairwise comparisons of the

historical series of T_s and σ_x during summer. The prominence of a peak measures how much the peak stands out due to its intrinsic height and its location relative to other peaks.

For both variables, cooler colors (smaller differences) dominate comparisons between temporally close years, while warmer colors (larger positive differences) become more frequent as the temporal gap increases. Notably, years after 2018 tend to exhibit higher positive differences when compared to the early years of the series, indicating an intensification of extreme events in recent summers.

The scatters plots in Fig. 4 present an integrated analysis of the temporal similarity and morphological variation of hourly summer series. It is observed that peak magnitude and daily cycle shape do not vary in a fully dependent manner. Some cases show increased peak intensity without significant temporal shifts, while others exhibit changes in daily profile shape without large amplitude variations.

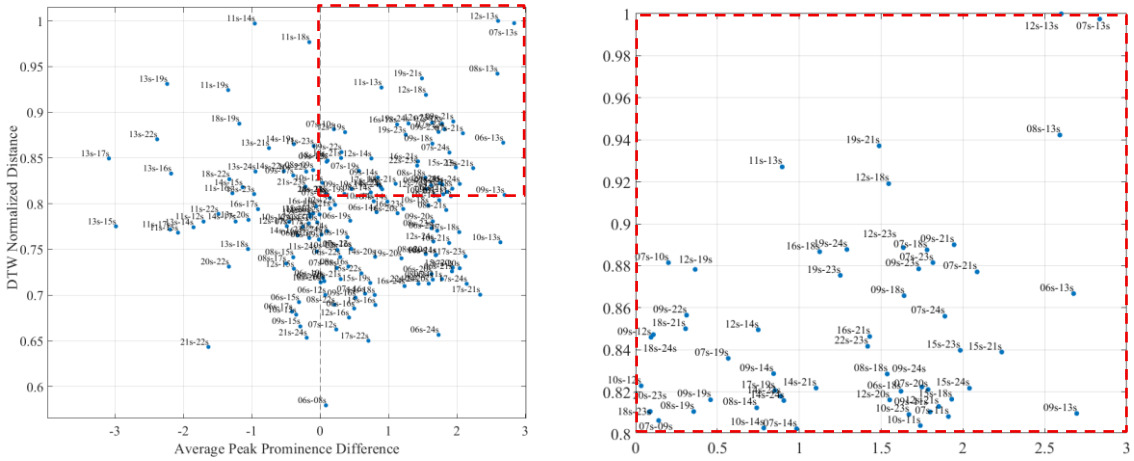
For comparisons with high X and Y for T_s (Fig. 4a), there is a noticeable recurrence of older years in the second term of the pair (e.g., 07s–13s, 08s–13s). This pattern suggests that, for these combinations, there were both greater differences in peak magnitude and perceptible changes in the daily temperature curve shape. Comparisons involving the year 2013 stand out for exhibiting large absolute values of peak prominence difference, both positive and negative, indicating that this year's summers had markedly different peak patterns compared to many others.



(a) (b)

Figure 3. Heat map of comparison between summer series: (a) average peak prominence difference for T_s series; and (b) average peak prominence difference for σ_x series.

The results for the hourly σ_x stress series (Fig. 4b) show that, although most year-to-year comparisons present moderate DTW distances (0.7-0.8), indicating relatively similar daily stress patterns, specific pairs, particularly those involving 2020, exhibit higher DTW values, reflecting significant changes in the temporal shape of the daily stress cycle. Analyzing the peak prominence mean difference map, this observation is confirmed, with 2020 standing out for its high absolute values when compared to several other years.



(a)

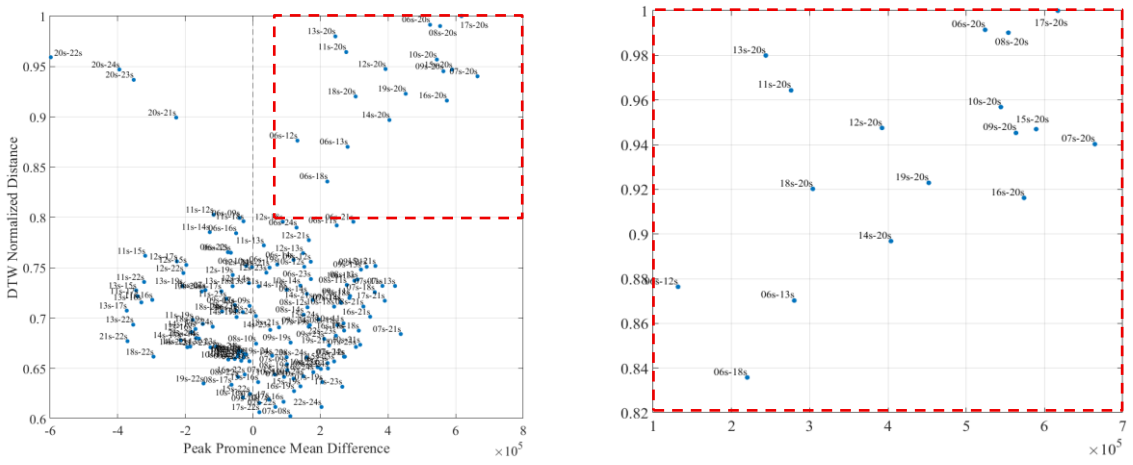


Figure 4. Scatter plot of normalized DTW distance versus average peak prominence difference (a) for T_s and (b) for σ_x.

As observed for the T_s series, the σ_x scatter plot shows that changes do not always coincide: some cases have high prominence with low DTW, while others show the opposite, highlighting the importance of jointly evaluating both metrics to characterize the evolution of thermally induced stress.

5 Conclusions

The analysis of almost two decades of hourly climatic data indicates a persistent increase in seasonal pavement surface temperatures and stresses. Variations in thermal gradients have resulted in increased curling stresses, with pronounced anomalies observed in specific years, particularly 2013 and 2020. The combined DTW and prominence approach proved effective in distinguishing magnitude changes from shifts in daily cycle shape, providing a more comprehensive understanding of the climatic impacts on rigid pavements. This distinction is relevant for pavement engineering, as shifts in peak timing can alter vertical thermal gradients, while changes in magnitude directly affect the maximum stresses applied to the material.

Acknowledgements. The authors gratefully acknowledge the financial support granted by the Brazilian foundation CAPES (Brazilian Federal Agency for Support and Evaluation of Graduate Education) and the general support and research incentive of University of Brasília.

Authorship statement. The authors hereby confirm that they are the sole liable persons responsible for the authorship of this work, and that all material that has been herein included as part of the present paper is either the property (and authorship) of the authors, or has the permission of the owners to be included here.

References

[1] M. Solaimanian and T. W. Kennedy, "Predicting maximum pavement surface temperature using maximum air temperature and hourly solar radiation", *Journal of the Transportation Research Board,* vol. 1417, pp. 1-11., 1993.
[2] R. Geiger, *The climate near the ground*, Harvard University Press, Cambridge, Mass., 1959.
[3] Y. Qin and J. E. Hiller, "Modeling temperature distribution in rigid pavement slabs: Impact of air temperature", *Construction and Building Materials*, vol. 25, pp. 3753-3761, 2011.
[4] Y. H. Huang, Pavement Analysis and Design, 2nd ed. Upper Saddle River, NJ, USA: Pearson Prentice Hall, 2004.
[5] H. Sakoe and S. Chiba, Dynamic programming algorithm optimization for spoken word recognition," *IEEE Transactions on Acoustics, Speech, and Signal Processing*, vol. 26, no. 1, pp. 43–49, 1978.
[6] M. Müller, *Information Retrieval for Music and Motion*. Berlin, Heidelberg: Springer, 2007.
[7] Instituto Nacional de Meteorologia (INMET), Available: https://portal.inmet.gov.br/. [Accessed: Apr. 12, 2025]
[8] Chartered Institution of Building Services Engineers (CIBSE), "Guide A: Environmental Design".
[9] Federal Highway Administration (FHWA), "Thermal properties of concrete pavements". Available: https://www.fhwa.dot.gov/publications/research/infrastructure/pavements/pccp/thermal.cfm. [Accessed: Jul. 19, 2025].